Mesozoic 001 (3): 264–275
https://www.mapress.com/mz/

Article

ISSN 3021-1859 (print edition)
MESOZOIC
ISSN 3021-1867 (online edition)

https://doi.org/10.11646/mesozoic.1.3.6
http://zoobank.org/urn:lsid:zoobank.org:pub:8429B693-6209-4A55-B257-09764CBB056F

New zircon U-Pb age of the top Duoni Formation, Basu County: constraits on the collision between Qiangtang and Lhasa blocks in Eastern Tibet

YONG ZHANG[1], HAI-LONG GAO[2], REN-BO HUANG[3], YI-TONG SU[1], YAN-ZHE FU[1], CHEN-YANG CAI[1] & DI-YING HUANG[1,*]

[1]*State Key Laboratory of Palaeobiology and Stratigraphy, Nanjing Institute of Geology and Palaeontology, Chinese Academy of Sciences, Nanjing 210008, China*
[2]*School of Earth Sciences, East China University of Technology, Nanchang, Jiangxi 330013, China*
[3]*School of Resources and Environment, Xichang University, Xichang 615000, China*
yzhang@nigpas.ac.cn; https://orcid.org/0000-0001-8237-6498
cugloong@163.com; https://orcid.org/0000-0002-6365-9983
dg1629014@smail.nju.edu.cn; https://orcid.org/0000-0002-1347-055X
ytsu@nigpas.ac.cn; https://orcid.org/0000-0003-0547-0792
yzfu@nigpas.ac.cn; https://orcid.org/0000-0002-7819-1703
cycai@nigpas.ac.cn; https://orcid.org/0000-0002-9283-8323
dyhuang@nigpas.ac.cn; https://orcid.org/0000-0002-5637-4867
**Corresponding author*

Abstract

The Duoni Formation is widely distributed along the Bangong-Nujiang suture belt and surrounding blocks in Tibet, serving as a key sedimentary record of the collision between the Qiangtang and Lhasa blocks. The upper sections of the formation typically contain andesite, volcanic rocks and tuff offering potential for precise stratigraphic correlations across the suture belt. The Duoni Formation in the central and western belt has been well-constrained geochronologically through zircon U-Pb dating; however, the insufficient age constraints on Duoni Formation in eastern Tibet hinder effective stratigraphic correlation and limit the understanding of the timing of this collision. Building on prior stratigraphic and paleontological studies, we collected three tuff samples from the upper Duoni Formation at the Wada coal mine section in Basu County, eastern Tibet. Zircon U-Pb dating was used to determine the age of the Duoni Formation, yielding results of 112.8 ± 1.0 Ma for sample XZ01, 111.48 ± 0.37 Ma for sample XZ03, and 110.95 ± 0.41 Ma for sample XZ05. These absolute ages correspond with early Albian and are generally consistent with those absolute ages from the central and western suture belt. Our study therefore suggests the similar timing for the Qiangtang-Lhasa collision across the whole Bangong-Nujiang belt.

Keywords: Early Cretaceous, Aptain–Albian, Bangong-Nujiang belt, Zircon U-Pb

Introduction

The Bangong-Nujiang (BN) suture zone is a crucial tectonic belt marking the collision between the Qiangtang and Lhasa blocks. Geological studies in this region have significantly advanced our understanding of the tectonic evolution of the Tibet (Girardeau *et al*., 1984). The volcanic-sedimentary rocks of the Duoni Formation are often associated with this collision, and their ages provide important insights into the closure of the BN Tethyan Ocean and the subsequent collision between the two blocks (Li *et al*., 2020; Zhu *et al*., 2022). In the central and western parts of the BN belt, ziron U-Pb dating has well-constrined the age of the Duoni Formation to approximately 110–125 Ma (Kapp *et al*., 2005; Zhu *et al*., 2019, 2020, 2022). Paleontological evidence, such as the discovery of *Neithea nipponica Hayami* from the sandstones of the Duoni Formation in Gerze (western BN belt), supports a late Early Cretaceous Aptian–Albian age (Zhang *et al*., 2019).

Despite extensive research in the western and central parts of the BN belt, the eastern segment remains insufficiently explored and lacks definitive conclusions. Although detrital zircon analyses and zircon age constraints from a volcanic rock have been conducted for the Duoni Group in eastern Tibet, more age constraints are generally needed for verification, particularly from tuff (Yin *et al*., 2024). Plant fossils discovered in the

 Submitted: 31 Aug. 2024; accepted by Z. Feng: 18 Sept. 2024; published: 26 Sept. 2024

Duoni Formation of eastern Tibet (Chen *et al*., 1983) suggest a possible age range, but the lack of precise dating limits our understanding of these critical geological processes. This study addresses this gap by conducting zircon U-Pb dating on tuff samples from the upper Duoni Formation in eastern Tibet. The goals are to constrain the formation's age more precisely, strengthen stratigraphic correlations with other Tibetan Plateau strata, and provide further insights into the collision between the Lhasa and Qiangtang blocks

Geological setting

The BN suture zone is a more than 1500 km long east-west oriented belt located in central Tibet (Ma *et al*., 2023; Taylor *et al*., 2003). This suture zone is divided into three segments: the western section, spanning from Bangong Lake to Gerze; the central section, spanning from Amdo to Dongqiao; and the eastern section, spanning from Dingqing to the Nujiang River (Fan *et al*., 2015; Hu *et al*., 2022). The BN suture formed due to the closure of the Tethys Ocean, which separated the Qiangtang Block from the Lhasa Block (Wang *et al*., 2016). The Duoni Formation, extensively distributed along the BN belt, was named in 1962 by Si Xingjian and Zhou Zhiyan. Its lower section typically consists of interbedded calcareous sandstone, shale, and siltstone. The middle section is characterized by sandstone and black shale, while the upper section contains dacite, andesite, sandstone, marl, clastic rocks, and tuff. Coal seams are commonly found throughout the formation (Zhou *et al*., 2000). Biostratigraphically, the Duoni Formation contains a variety of plant fossils, including *Zamiophyllum buchianum*, *Weichselia reticulata*, *Cladophlebis* sp., *Klukia browniana, Glossozamites* sp., *Onychiopsis* sp., *O. elongata, Nilssonia* sp., *and Sphenopteris* sp. Additionally, bivalve fossils such as *Velsella cf. imbricata*, *Chlamys cf. ineaquicostata, Astarte* sp., *and Pseudotrapezium* sp., along with ammonites and crinoids, have been found. These fossils generally suggest a broad age range for the Duoni Formation, from the late Jurassic to the early Cretaceous (Chen & Yang, 1982). Zircon U-Pb dating on dacite, andesite, and tuff from the upper Duoni Formation in the central and western parts of the BN belt has yielded age range from 110–125 Ma (Kapp *et al.*, 2005; Sun *et al.*, 2017; Zhu *et al.*, 2019).

In eastern Tibet, the age of the Duoni Formation has primarily been constrained by plant fossils (*e.g. Zamiophyllum-Weichselia-Klukia*), indicating a relatively broad time span in Neocomian (Chen *et al*., 1983). In the Wada coal section (GPS: 97° 06′ 39″; 30° 00′ 12″), the lower Duoni Formation consists of interbedded quartz sandstone, siltstone and shale, while the upper part comprises quartz sandstone and carbonaceous shale. The topmost layer contains andesite, quartz sandstone, volcanic rocks and tuff, with over 30 coal seams present throughout the section (Wu, 1985; Yin *et al.*, 2024). Numerous plant fossils have been discovered within this lithostratigraphic unit (Li, 1982), including *Klukia* sp., *Zamiophyllum buchianum* (Ett.), *Weichselia reticulata* (S. & W.), *Sphenopteris cretacea* Li, *Gleichenites* sp., *Sagenopteris* sp., *Pseudotenis* sp., *Taeniopteris* sp., *Frenelopsis* sp., *Cladophlebis* cf. *browniana* Lee, *Ptilophyllum* sp., *Podozamites* sp., *Zamites* cf. *niumagouensis* Wu. Comparison of these plant assemblages with both domestic and international references suggests that this section corresponds to the Early Cretaceous.

Materials and methods

Sampling

To constrain the age of Duoni Formation in the Eastern Tibet, three tuff samples (XZ01, 03, 05) were collected from the top of Duoni Formation in the Wada coal section in Basu County (GPS: 97° 06′ 39″; 30° 00′ 12″; Fig. 1). Based on the relative positioning within the stratigraphy, XZ01 is lower, XZ03 is in the middle, and XZ05 is higher. Thin sections were prepared for the samples and examined under an optical microscope to analyse their microscopic composition and structure, confirming the rock type. Zircons were isolated from the crushed tuff samples by hand-picking for the preparation of the analytical target, and then the target zircon was photographed to obtain transmitted light and reflected light at the Hebei Langfang Chengxin Geological Service Co., LTD. Target zircons were also photographed to obtain cathodic luminescence (CL) images in the State Key Laboratory of Continental Dynamics, Northwest University. Zircon U-Pb dating spots were selected according to their images to avoid defects and carried out dating analysis.

Dating

We performed zircon U-Pb dating of tuff samples by LA-ICP-MS at the State Key Laboratory of Continental Dynamics, Northwest University, Xi'an, China, and zircon U-Pb isotopes were analysed by Agilent 7500a inductively coupled plasma mass spectrometer and Lambda Physik Geolas 193 nm laser ablation system. The age and element content of U-Pb were calculated by Glitter (ver. 4.0) (Košler, 2007). Zircon standard 91500 and GJ-1 were used as independent controls to analyse reproducibility and instrument stability for every 6 sample zircons. The Excel program ComPbCorr#3_15G was used for ordinary Pb correction. U-Pb age calculations,

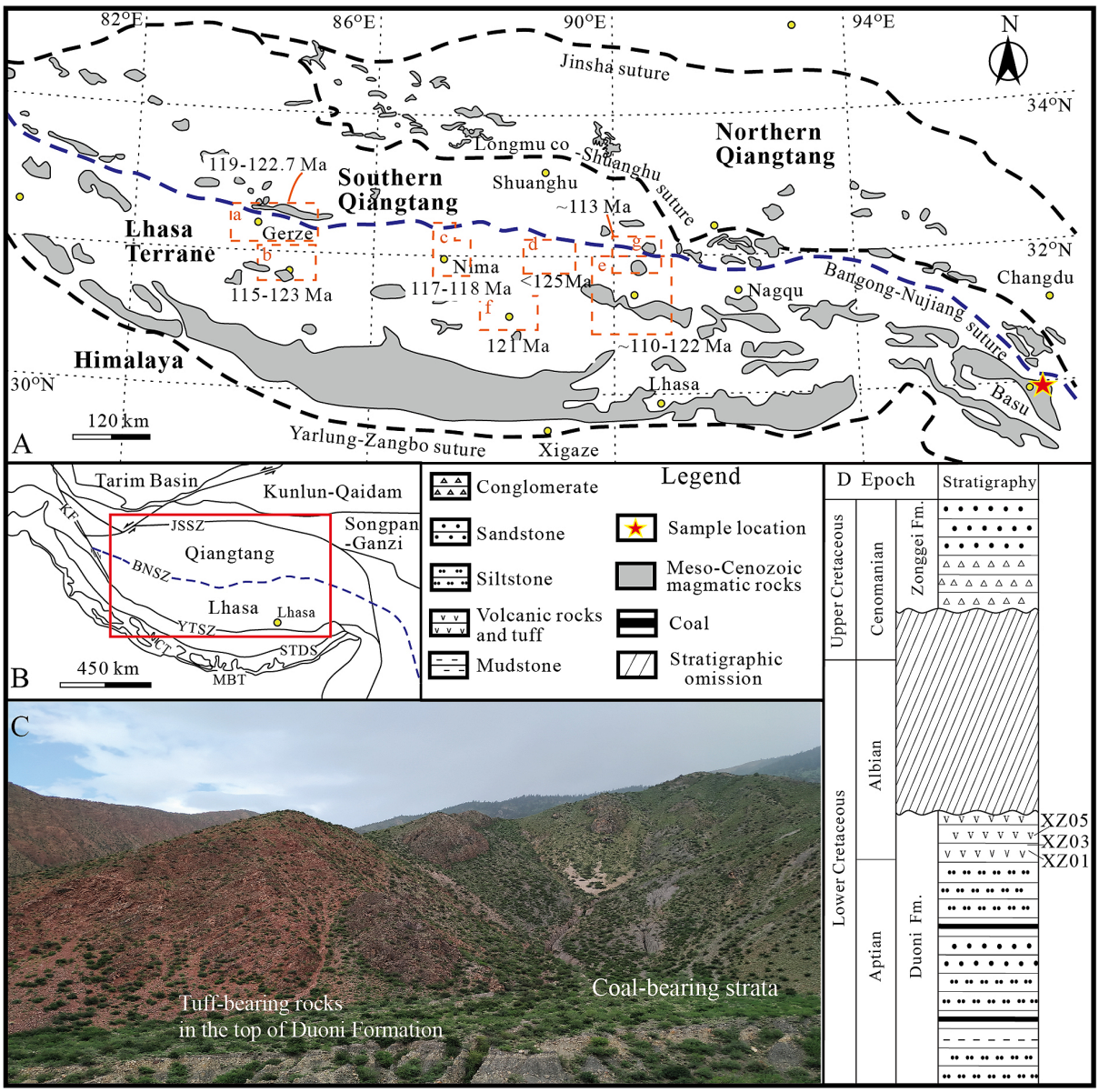

FIGURE 1. Geological sketch map showing the Bangong-Nujiang Suture Zone and the surrounding Qiangtang and Lhasa blocks (modified from Li *et al*., 2020), along with sampling locations. **A**, Illustrates the distribution of Mesozoic-Cenozoic igneous rocks (grey areas) and previous dating work in the central and western BN belt (orange dashed rectangles), with the pentagrams representing the sampling locations in this study. The studies are labelled as follows: a (Li *et al.*, 2020); b (Sun *et al.*, 2017); c (Kapp *et al*., 2007); d (Zhang *et al.*, 2011); e (Lai *et al.*, 2019); f (Fan *et al.*, 2017); g (Zhu *et al.*, 2022). **B**, A geological sketch map of the Tibetan Plateau, with the red box indicating the area shown in **A**. **C**, the outcrop figure shows the top of the Duoni Formation with tuff strata and the coal-bearing strata below. **D**, The stratigraphic column of the sampling section.

concordant graphs and isogram probability curves were created by isoplot (version 4.0).

Results

Characteristics observed under the thin section microscope

Sample XZ01 is primarily composed of crystal fragments (including quartz, feldspar, and a small amount of mica), magma fragments, and a few lithic fragments (>2mm as breccia; Fig. 2). Quartz grains are sub-angular to sub-rounded and may have been subject to corrosion and make up about 30%. Some lithic fragments (Det) and magma fragments (Mf) are also present. The magma fragments have undergone plastic deformation, with some displaying torn ends or encapsulating rigid lithic fragments (A-1 and A-3). Volcanic ash is mostly distributed in the matrix. The rock is classified as a crystal tuff.

Sample XZ03 consists mainly of crystal fragments

(feldspar, quartz, and biotite), with volcanic ash as the primary matrix. Feldspar often shows polysynthetic twinning and zoning. Quartz grains are mostly corroded and exhibit embayed shapes, which indicates their volcanic origin. Calcite veins are observed. Hematite (Hm) is distributed in the matrix. The volcanic ash in the matrix is devitrified.

Sample XZ05 consists mainly of lithic and crystal fragments (quartz, feldspar, and a small amount of mica). Feldspar commonly shows embayed shapes, and some particles are fragmented. Calcite veins are observed. Volcanic ash is primarily distributed in the matrix and is devitrified (Fig. 2).

Zircon U-Pb ages

The zircon particles extracted from the tuff samples are colourless and pan-faceted, with length of 50–200 μm and width of 20–120 μm. In the CL image (Fig. 3), most zircon grains show well-developed oscillating bands and are positive euhedral-subhedral crystals. The Th/U ratios of most zircon grains are more than 0.4 (Table 1), indicating that the zircons are of magmatic origin. All zircon U-Pb chronological analysis data are shown in Table 1. Zircons U-Pb ages are only discarded if they are highly inconsistent (*i.e.*, <95%).

Sample XZ01

Fouty-five grains were analysed, and 35 grains yielded concordia U-Pb ages. The youngest ages of the 11 zircons range from 110.3 ± 0.98 Ma to 115.1 ± 0.93 Ma, and they usually appear as euhedral-subhedral crystals with a weighted average of 112.8 ± 1.0 Ma (n = 11, Mean Square Weighted Deviation (MSWD) = 2.4; Fig. 4; Table 1), which was considered as the sedimentation ages of the Duoni Formation. The inherited zircons yielded concordia ages ranging from 434 Ma to 120 Ma.

Sample XZ03

Forty-five particles were analysed in sample XZ03. 34 zircons yield concordia U-Pb ages from 109.1 ± 1.08 to

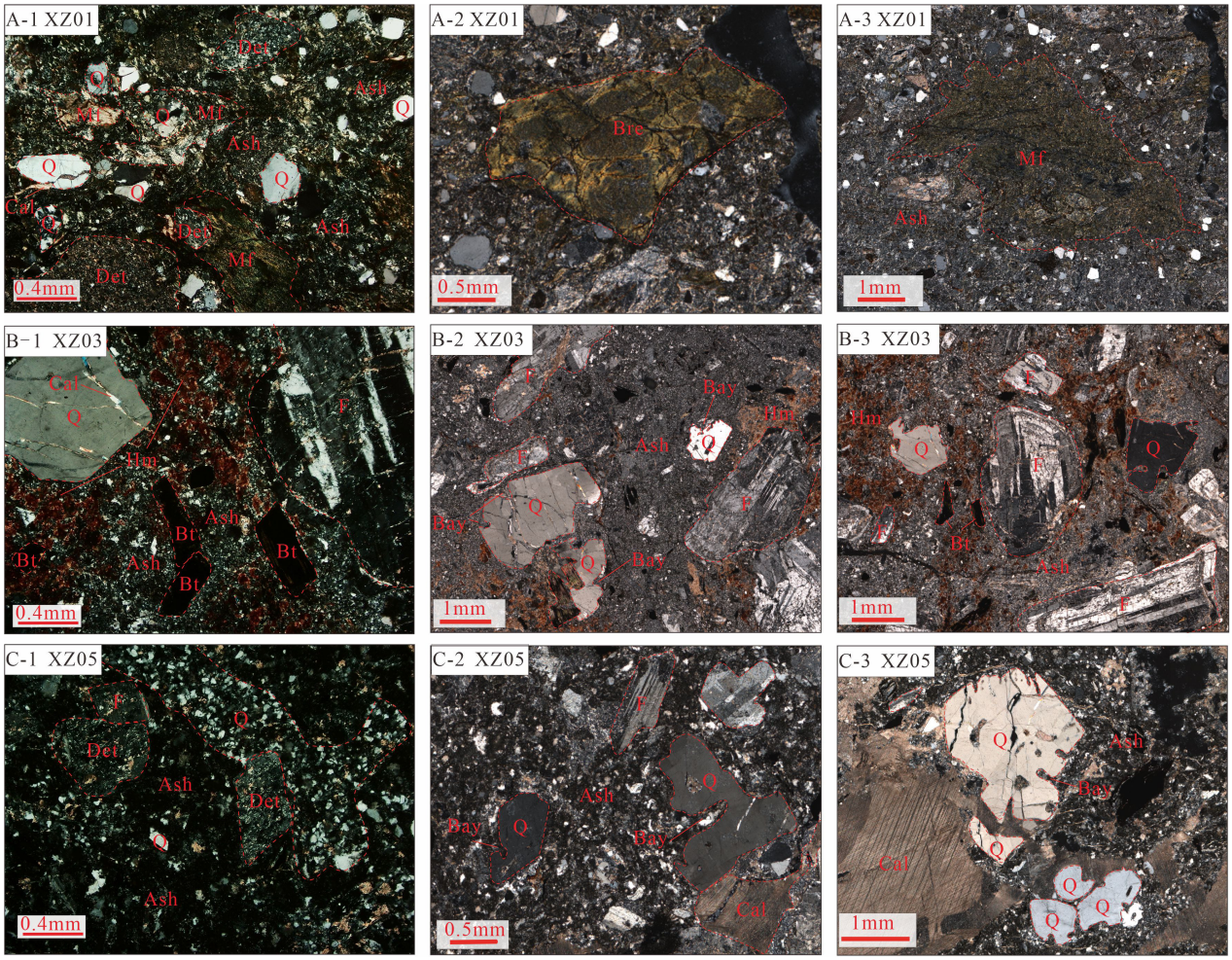

FIGURE 2. The microscopic characteristics of three tuff samples (A-1, -2, -3-XZ01; B-1, -2, -3-XZ03; C-1, -2, -3-XZ05), including microstructure, texture, mineral composition, and morphological features. Q, Quartz; F, Feldspar; L, Lithic fragments; Cal, Calcite vein; Det, Crystal fragment; PD, Magma fragment; Pl, Plagioclase; Ash, Volcanic ash; Hm, Hematite.

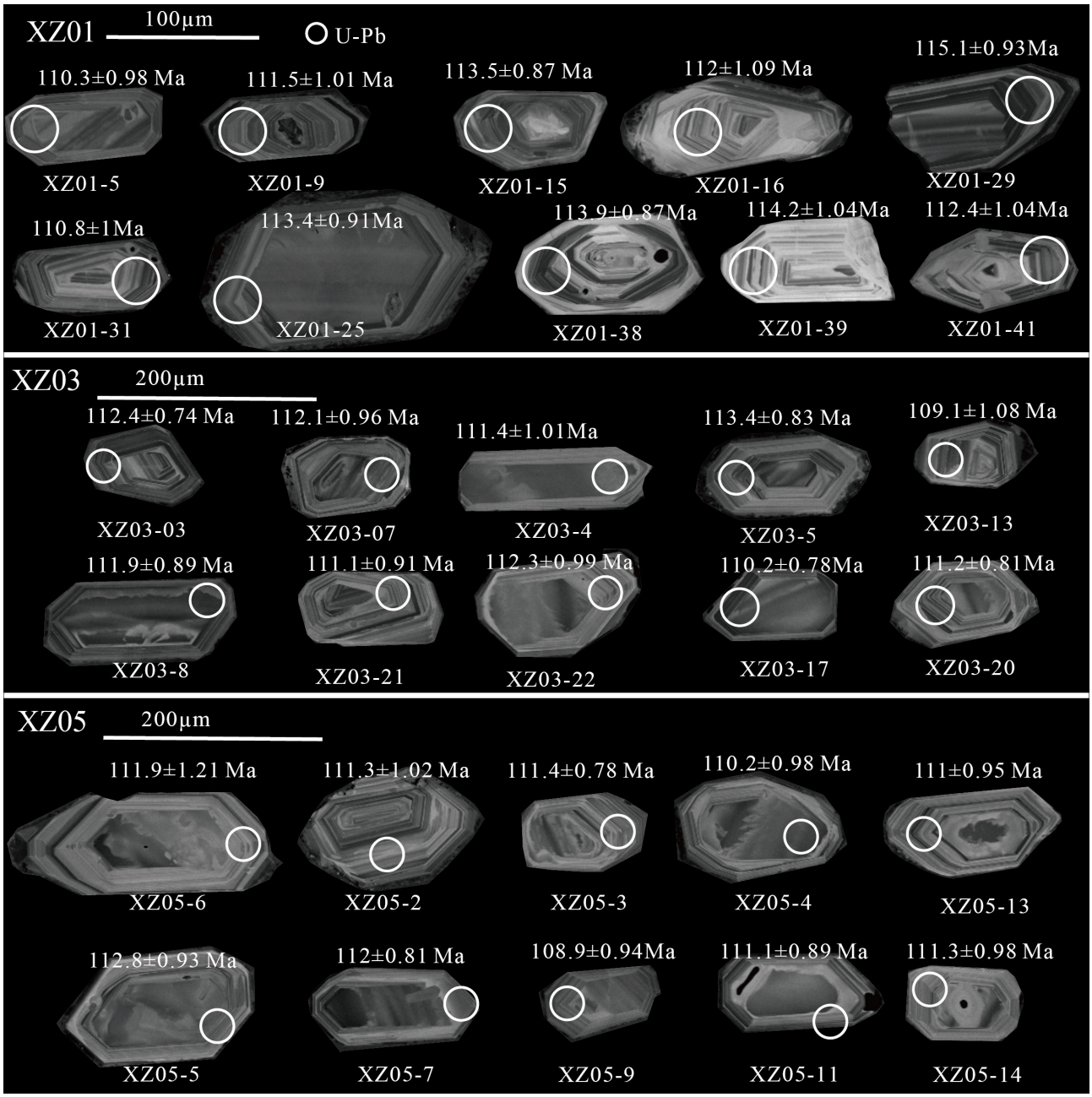

FIGURE 3. Representative CL images of zircons from the Duoni Formation in Basu County showing internal structure and morphology of zircons.

113.6 ± 1.06 Ma and are euhedral-subhedral crystals with a weighted mean of 111.48 ± 0.37 Ma (n = 34, MSWD = 1.4; Fig. 4; Table 1). The results show that the tuff was formed at 111.48 ± 0.37 Ma.

Sample XZ05

Thirty-two zircons were analysed. The 26 zircons have positive body-subhedral crystals with U-Pb ages ranging from 108.9 ± 0.94 Ma to 112.8 ± 0.9 Ma. The weighted mean age is 110.95 ± 0.41 Ma (n = 26, MSWD = 1.3; Fig. 4; Table 1). The results show that the tuff was formed at 110.95 ± 0.41 Ma

Discussion

Age of the Duoni Formation in eastern Tibet, stratigraphic correlation and tectonics

Zircon U-Pb dating of three tuff samples from the upper Duoni Formation in the Wada section reveals isotopic ages ranging from approximately 110.95 to 112.8 Ma. These dates align with palaeobotanical studies that suggest the Duoni Formaiton in eastern Tibet belongs to the Early Cretaceous.

Similarly, in the central and western areas near the BN belt, interbedded tuff zircon dating results from the

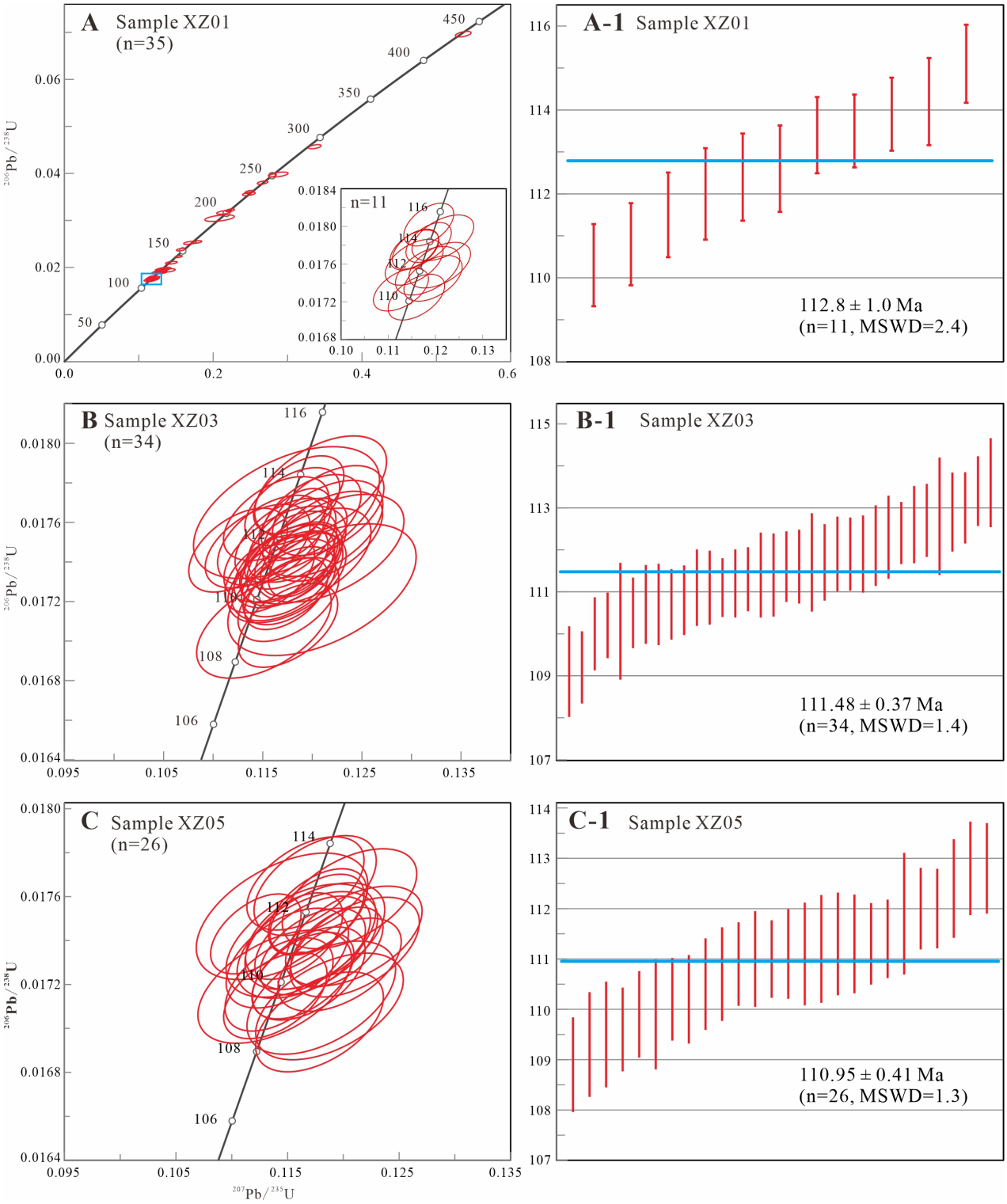

FIGURE 4. Concordia diagrams showing U-Pb age data for three zircon samples (XZ01, XZ03 and XZ05). Each diagram includes ellipses representing the uncertainty in the isotopic ratios and the corresponding concordia curves (**A**–**C**). A-1, B-1 and C-1 show the age distribution histograms for each sample, on the left with their respective MSWD values and calculated weighted mean ages. The ages are as follows: **A**, XZ01 with n=11 (112.8 ± 1.0 Ma). **B**, XZ03 with n=34 (111.48 ± 0.37 Ma). **C**, XZ05 with n=26 (110.95 ± 0.41 Ma).

Duoni Formation in the Coqên Basin of northern Lhasa are approximately 123–115 Ma (Sun *et al.*, 2017). In the Nima area, tuff dating results from the Duoni Formation are approximately 117–118 Ma (Kapp *et al.*, 2007). The dating results for the volcaniclastic rocks from the Duoni Formation around Nima are ~121 Ma (Fan *et al.*, 2015).

TABLE 1. LA-ICP-MS zircon U-Pb analyses for tuff samples from the Duoni Formation, Tibet.

Analysis	Pb* (ppm)	Th	U	Th/U	Isotopic ratios						Isotopic ages (Ma)						Concordance (%)
					$^{207}Pb/^{206}Pb$	1σ	$^{207}Pb/^{235}U$	1σ	$^{206}Pb/^{238}U$	1σ	$^{207}Pb/^{206}Pb$	1σ	$^{207}Pb/^{235}U$	1σ	$^{206}Pb/^{238}U$	1σ	
Sample XZ01																	
01	7	169	233	0.72	0.07004	0.00253	0.1878	0.00639	0.01945	0.0002	929.5	72.4	174.7	5.5	124.2	1.3	71
02	57	453	1040	0.44	0.05129	0.00077	0.27985	0.00337	0.03958	0.00022	253.9	34.2	250.5	2.7	250.2	1.4	100
03	14	305	373	0.82	0.06142	0.0015	0.20842	0.00465	0.02462	0.00018	653.9	51.7	192.2	3.9	156.8	1.1	82
04	21	304	339	0.90	0.05243	0.0017	0.28744	0.00882	0.03977	0.00035	304.2	72.3	256.5	7.0	251.4	2.2	98
05	16	650	636	1.02	0.04877	0.00175	0.11597	0.00395	0.01725	0.00016	136.8	82.1	111.4	3.6	110.3	1.0	99
06	7	106	184	0.57	0.04846	0.00168	0.16865	0.00554	0.02525	0.00022	121.9	79.6	158.2	4.8	160.7	1.4	98
07	45	219	476	0.46	0.0559	0.00089	0.5363	0.007	0.0696	0.0004	448.0	34.6	436.0	4.6	433.7	2.4	99
08	62	410	1223	0.34	0.05486	0.0008	0.28784	0.0033	0.03806	0.00021	406.4	32.0	256.9	2.6	240.8	1.3	94
09	23	271	678	0.40	0.04967	0.00178	0.1195	0.00407	0.01745	0.00016	179.7	81.6	114.6	3.7	111.5	1.0	97
10	37	573	705	0.81	0.05002	0.00093	0.2486	0.004	0.03605	0.00022	195.9	42.6	225.4	3.3	228.3	1.4	99
11	11	200	321	0.62	0.11493	0.00278	0.30882	0.00666	0.01949	0.00017	1878.9	43.0	273.3	5.2	124.4	1.1	46
12	6	86	251	0.34	0.04852	0.00185	0.12858	0.00467	0.01922	0.00018	124.6	87.3	122.8	4.2	122.7	1.1	100
13	28	403	619	0.65	0.05024	0.00098	0.2227	0.00383	0.03215	0.0002	206.0	44.8	204.2	3.2	204.0	1.3	100
14	9	161	334	0.48	0.06225	0.00176	0.16194	0.00425	0.01887	0.00015	682.6	59.4	152.4	3.7	120.5	1.0	79
15	12	199	511	0.39	0.04726	0.0014	0.11576	0.00322	0.01776	0.00014	62.1	69.7	111.2	2.9	113.5	0.9	98
16	9	168	346	0.49	0.04897	0.00195	0.11835	0.00449	0.01753	0.00017	146.4	90.6	113.6	4.1	112.0	1.1	99
17	9	186	353	0.53	0.04718	0.00158	0.12276	0.00388	0.01887	0.00016	58.1	78.2	117.6	3.5	120.5	1.0	98
18	4	38	134	0.28	0.0496	0.00321	0.2086	0.01312	0.0305	0.00046	176.4	144.4	192.4	11.0	193.7	2.9	99
19	11	201	235	0.85	0.04902	0.00154	0.21434	0.00636	0.03171	0.00026	148.9	72.1	197.2	5.3	201.2	1.7	98
20	5	98	195	0.50	0.04838	0.00224	0.12704	0.00567	0.01904	0.00021	117.7	105.8	121.4	5.1	121.6	1.3	100
21	21	343	400	0.86	0.05689	0.00137	0.27773	0.00612	0.0354	0.00026	486.8	52.5	248.9	4.9	224.3	1.6	90
22	7	218	246	0.89	0.04989	0.00194	0.1308	0.00485	0.01901	0.00019	190.0	88.0	124.8	4.4	121.4	1.2	97
23	32	144	523	0.28	0.05343	0.00103	0.33665	0.00571	0.04569	0.00029	347.0	43.2	294.6	4.3	288.0	1.8	98
24	6	116	212	0.55	0.05158	0.00291	0.13768	0.00751	0.01936	0.00026	266.7	124.5	131.0	6.7	123.6	1.6	94
25	12	394	458	0.86	0.0472	0.00148	0.11557	0.00341	0.01775	0.00014	59.1	73.4	111.0	3.1	113.4	0.9	98
26	21	692	591	1.17	0.04984	0.00116	0.15346	0.00323	0.02233	0.00015	187.4	53.1	145.0	2.9	142.3	1.0	98
27	6	163	193	0.85	0.04923	0.00234	0.13389	0.00614	0.01972	0.00022	158.6	107.7	127.6	5.5	125.9	1.4	99
28	27	306	496	0.62	0.05078	0.00102	0.26645	0.00475	0.03804	0.00024	230.7	45.8	239.8	3.8	240.7	1.5	100
29	19	457	745	0.61	0.04771	0.00149	0.11859	0.00349	0.01802	0.00015	84.3	73.5	113.8	3.2	115.1	0.9	99
30	6	159	222	0.72	0.04962	0.002	0.12956	0.005	0.01893	0.00018	177.3	91.4	123.7	4.5	120.9	1.2	98
31	14	695	506	1.38	0.04714	0.00169	0.1127	0.00385	0.01733	0.00015	55.8	83.9	108.4	3.5	110.8	1.0	98
32	4	62	147	0.42	0.06893	0.00327	0.19416	0.00881	0.02042	0.00026	896.5	94.9	180.2	7.5	130.3	1.6	72
33	8	149	287	0.52	0.04899	0.00215	0.13182	0.00555	0.01951	0.00021	147.2	99.7	125.7	5.0	124.5	1.3	99
34	13	206	391	0.53	0.04766	0.00128	0.15647	0.0039	0.0238	0.00018	81.4	63.4	147.6	3.4	151.6	1.1	97
35	16	87	356	0.24	0.05044	0.00126	0.24805	0.0057	0.03566	0.00026	215.2	57.0	225.0	4.6	225.9	1.6	100
36	8	164	254	0.65	0.04962	0.00188	0.14376	0.00518	0.02101	0.0002	177.3	85.9	136.4	4.6	134.0	1.2	98
37	25	159	392	0.40	0.06476	0.00128	0.3947	0.00682	0.0442	0.0003	766.5	41.0	337.8	5.0	278.8	1.8	83
38	12	182	523	0.35	0.04822	0.00138	0.11856	0.00317	0.01783	0.00014	110.1	66.3	113.8	2.9	113.9	0.9	100
39	8	297	297	1.00	0.04932	0.00184	0.12158	0.00431	0.01788	0.00016	163.0	84.8	116.5	3.9	114.2	1.0	98
40	12	154	183	0.84	0.09705	0.00233	0.51178	0.01106	0.03824	0.00033	1568.2	44.4	419.6	7.4	241.9	2.0	58
41	8	221	315	0.70	0.04986	0.00186	0.12092	0.0043	0.01759	0.00016	188.3	84.7	115.9	3.9	112.4	1.0	97
42	17	491	412	1.19	0.05071	0.00139	0.17785	0.00453	0.02543	0.00019	227.9	62.1	166.2	3.9	161.9	1.2	97
43	6	118	218	0.54	0.0481	0.00197	0.12989	0.00511	0.01958	0.00019	104.1	94.3	124.0	4.6	125.0	1.2	99
44	3	61	69	0.89	0.06753	0.0036	0.24341	0.01252	0.02614	0.00036	854.1	107.1	221.2	10.2	166.3	2.2	75
45	14	607	493	1.23	0.04753	0.00174	0.11551	0.00404	0.01762	0.00016	75.3	85.7	111.0	3.7	112.6	1.0	99

.....continued on the next page

TABLE 1. (Continued)

Analysis	Pb* (ppm)	Th	U	Th/U	Isotopic ratios						Isotopic ages (Ma)						Concordance (%)
					$^{207}Pb/^{206}Pb$	1σ	$^{207}Pb/^{235}U$	1σ	$^{206}Pb/^{238}U$	1σ	$^{207}Pb/^{206}Pb$	1σ	$^{207}Pb/^{235}U$	1σ	$^{206}Pb/^{238}U$	1σ	
Sample XZ03																	
01	12	330	477	0.69	0.05502	0.00187	0.12849	0.00412	0.01693	0.00015	413.0	73.6	122.7	3.7	108.3	1.0	88
02	14	395	595	0.66	0.05346	0.00137	0.12591	0.00296	0.01708	0.00013	348.1	56.9	120.4	2.7	109.2	0.8	91
03	25	900	938	0.96	0.04875	0.0011	0.11826	0.00242	0.01759	0.00012	136.0	52.4	113.5	2.2	112.4	0.7	99
04	13	595	482	1.24	0.04978	0.00181	0.11965	0.00414	0.01743	0.00016	184.5	82.7	114.8	3.8	111.4	1.0	97
05	15	422	594	0.71	0.04848	0.00133	0.11863	0.00301	0.01774	0.00013	122.8	63.2	113.8	2.7	113.4	0.8	100
06	12	301	423	0.71	0.06062	0.00186	0.14721	0.00421	0.01761	0.00015	625.8	64.7	139.4	3.7	112.5	1.0	81
07	13	372	519	0.72	0.05018	0.00166	0.12134	0.00379	0.01753	0.00015	203.5	75.1	116.3	3.4	112.1	1.0	96
08	12	355	480	0.74	0.04859	0.00148	0.11729	0.00336	0.01751	0.00014	127.9	70.3	112.6	3.1	111.9	0.9	99
09	9	219	340	0.64	0.05676	0.00191	0.14094	0.00447	0.018	0.00016	481.7	73.4	133.9	4.0	115.0	1.0	86
10	8	237	318	0.74	0.04876	0.00178	0.11724	0.00406	0.01744	0.00016	136.4	83.5	112.6	3.7	111.4	1.0	99
11	17	317	506	0.63	0.05023	0.00136	0.15532	0.0039	0.02242	0.00017	205.5	61.7	146.6	3.4	143.0	1.1	98
12	12	326	486	0.67	0.0493	0.00146	0.11988	0.00332	0.01763	0.00014	162.1	67.8	115.0	3.0	112.7	0.9	98
13	10	228	356	0.64	0.04892	0.00199	0.11512	0.00448	0.01707	0.00017	144.0	92.9	110.6	4.1	109.1	1.1	99
14	22	810	928	0.87	0.04905	0.0011	0.11157	0.00226	0.01649	0.00011	150.4	51.8	107.4	2.1	105.5	0.7	98
15	9	187	354	0.53	0.05051	0.00215	0.12171	0.00497	0.01747	0.00018	218.4	95.8	116.6	4.5	111.7	1.2	96
16	6	153	235	0.65	0.05081	0.00273	0.12098	0.00627	0.01726	0.00022	232.4	119.4	116.0	5.7	110.3	1.4	95
17	18	627	722	0.87	0.04938	0.00127	0.11738	0.00277	0.01724	0.00012	165.7	58.8	112.7	2.5	110.2	0.8	98
18	14	497	556	0.89	0.04992	0.00162	0.1216	0.00371	0.01766	0.00015	191.5	73.7	116.5	3.4	112.9	0.9	97
19	14	404	602	0.67	0.05029	0.00145	0.11853	0.00318	0.01709	0.00013	208.6	65.4	113.7	2.9	109.2	0.8	96
20	15	590	585	1.01	0.04883	0.00132	0.11713	0.00294	0.01739	0.00013	139.9	62.3	112.5	2.7	111.2	0.8	99
21	13	373	526	0.71	0.04899	0.00156	0.11743	0.00352	0.01738	0.00014	147.3	73.0	112.7	3.2	111.1	0.9	99
22	10	303	385	0.79	0.04997	0.00174	0.12106	0.004	0.01757	0.00016	193.7	79.1	116.0	3.6	112.3	1.0	97
23	15	373	631	0.59	0.04892	0.00137	0.11781	0.00306	0.01746	0.00013	144.2	64.2	113.1	2.8	111.6	0.8	99
24	13	517	494	1.05	0.04908	0.00146	0.1185	0.0033	0.01751	0.00014	151.8	68.3	113.7	3.0	111.9	0.9	98
25	10	309	385	0.80	0.0475	0.00153	0.11449	0.00349	0.01748	0.00014	73.7	75.7	110.1	3.2	111.7	0.9	99
26	15	540	576	0.94	0.0499	0.0015	0.11755	0.00331	0.01708	0.00014	190.6	68.5	112.8	3.0	109.2	0.9	97
27	38	2072	1390	1.49	0.04936	0.00099	0.11333	0.002	0.01665	0.0001	164.8	46.2	109.0	1.8	106.4	0.7	98
28	19	658	732	0.90	0.04942	0.00118	0.11868	0.00258	0.01741	0.00012	167.7	54.9	113.9	2.3	111.3	0.8	98
29	10	211	389	0.54	0.04917	0.00164	0.11747	0.00371	0.01733	0.00015	155.7	76.4	112.8	3.4	110.7	0.9	98
30	10	245	265	0.92	0.13276	0.00353	0.36715	0.00875	0.02005	0.0002	2134.8	45.8	317.5	6.5	128.0	1.3	40
31	11	302	451	0.67	0.04917	0.0015	0.11793	0.00337	0.01739	0.00014	156.0	69.9	113.2	3.1	111.1	0.9	98
32	13	352	480	0.73	0.04674	0.00145	0.11252	0.00329	0.01746	0.00014	35.6	73.0	108.3	3.0	111.6	0.9	97
33	9	185	340	0.54	0.04918	0.00174	0.11745	0.00394	0.01732	0.00015	156.3	80.7	112.8	3.6	110.7	1.0	98
34	11	295	461	0.64	0.04954	0.00151	0.1176	0.00336	0.01721	0.00014	173.5	69.6	112.9	3.1	110.0	0.9	97
35	13	418	517	0.81	0.04787	0.00153	0.11635	0.00351	0.01762	0.00014	91.8	75.2	111.8	3.2	112.6	0.9	99
36	10	229	375	0.61	0.06194	0.00192	0.15061	0.00437	0.01763	0.00015	672.0	65.1	142.4	3.9	112.7	1.0	79
37	12	272	483	0.56	0.04839	0.00139	0.11799	0.00316	0.01768	0.00013	118.2	66.3	113.3	2.9	113.0	0.9	100
38	14	379	524	0.72	0.04937	0.00139	0.11767	0.00308	0.01728	0.00013	165.4	64.6	113.0	2.8	110.5	0.8	98
39	9	195	318	0.61	0.05164	0.00234	0.12376	0.00539	0.01738	0.00019	269.4	100.7	118.5	4.9	111.1	1.2	94
40	25	890	1049	0.85	0.04838	0.00134	0.1157	0.00299	0.01734	0.00013	118.0	64.2	111.2	2.7	110.8	0.8	100
41	14	410	574	0.72	0.04796	0.00156	0.11584	0.00356	0.01751	0.00015	96.2	76.4	111.3	3.2	111.9	0.9	99
42	13	400	549	0.73	0.04921	0.0014	0.11757	0.00311	0.01732	0.00013	157.7	65.1	112.9	2.8	110.7	0.8	98
43	4	142	165	0.86	0.04824	0.00263	0.1174	0.00619	0.01765	0.00022	110.9	123.9	112.7	5.6	112.8	1.4	100
44	29	845	1180	0.72	0.0496	0.00104	0.11891	0.0022	0.01739	0.00011	176.1	48.0	114.1	2.0	111.1	0.7	97
45	8	208	333	0.62	0.04928	0.00188	0.12084	0.00439	0.01778	0.00017	161.3	86.7	115.8	4.0	113.6	1.1	98

.....continued on the next page

TABLE 1. (Continued)

Analysis	Pb* (ppm)	Th	U	Th/U	Isotopic ratios						Isotopic ages (Ma)						Concordance (%)
					$^{207}Pb/^{206}Pb$	1σ	$^{207}Pb/^{235}U$	1σ	$^{206}Pb/^{238}U$	1σ	$^{207}Pb/^{206}Pb$	1σ	$^{207}Pb/^{235}U$	1σ	$^{206}Pb/^{238}U$	1σ	
Sample XZ05																	
01	12	350	469	0.75	0.05105	0.00171	0.12021	0.00381	0.01708	0.00015	242.9	75.5	115.3	3.5	109.2	0.9	95
02	10	294	420	0.70	0.0489	0.00181	0.11745	0.00414	0.01742	0.00016	143.1	84.8	112.8	3.8	111.3	1.0	99
03	18	524	733	0.72	0.04667	0.00121	0.11216	0.00268	0.01743	0.00012	32.4	60.0	107.9	2.5	111.4	0.8	97
04	15	421	596	0.71	0.04895	0.00137	0.11638	0.00302	0.01724	0.00013	145.3	64.2	111.8	2.8	110.2	0.8	99
05	11	411	427	0.96	0.04825	0.00158	0.11747	0.00362	0.01765	0.00015	111.5	75.4	112.8	3.3	112.8	0.9	100
06	8	241	320	0.75	0.04741	0.00219	0.11451	0.00508	0.01751	0.00019	69.4	106.8	110.1	4.6	111.9	1.2	98
07	14	331	539	0.61	0.04868	0.0013	0.11769	0.00291	0.01753	0.00013	132.3	61.6	113.0	2.6	112.0	0.8	99
08	15	471	594	0.79	0.04915	0.0015	0.1169	0.00334	0.01725	0.00014	155.1	69.8	112.3	3.0	110.2	0.9	98
09	12	345	481	0.72	0.05019	0.0017	0.11787	0.00378	0.01703	0.00015	203.6	76.9	113.1	3.4	108.9	0.9	96
10	18	630	590	1.07	0.07166	0.00177	0.16935	0.0038	0.01714	0.00013	976.4	49.7	158.9	3.3	109.5	0.8	69
11	12	346	466	0.74	0.0489	0.00152	0.11725	0.00342	0.01739	0.00014	143.2	71.2	112.6	3.1	111.1	0.9	99
12	15	401	612	0.66	0.05063	0.00138	0.12053	0.00305	0.01726	0.00013	223.8	62.0	115.6	2.8	110.3	0.8	95
13	11	253	447	0.57	0.05053	0.00169	0.12101	0.00383	0.01737	0.00015	219.5	75.8	116.0	3.5	111.0	1.0	96
14	8	186	308	0.60	0.05034	0.00177	0.12094	0.00404	0.01742	0.00015	210.7	79.7	115.9	3.7	111.3	1.0	96
15	10	218	433	0.50	0.05393	0.00169	0.12949	0.00382	0.01741	0.00015	368.1	69.1	123.6	3.4	111.3	0.9	90
16	20	598	729	0.82	0.08169	0.0018	0.19574	0.00382	0.01738	0.00013	1238.1	42.4	181.5	3.3	111.0	0.8	61
17	26	836	1039	0.80	0.04817	0.00144	0.11424	0.0032	0.0172	0.00014	107.5	69.2	109.8	2.9	109.9	0.9	100
18	10	221	328	0.67	0.09561	0.00279	0.24975	0.00667	0.01894	0.00018	1540.1	53.8	226.4	5.4	121.0	1.2	53
19	14	336	576	0.58	0.04817	0.00139	0.11391	0.00306	0.01715	0.00013	107.8	66.6	109.5	2.8	109.6	0.8	100
20	11	409	420	0.97	0.04873	0.00183	0.11678	0.00416	0.01738	0.00016	134.9	85.7	112.2	3.8	111.1	1.0	99
21	9	215	354	0.61	0.04844	0.00193	0.1162	0.00443	0.0174	0.00017	120.7	91.3	111.6	4.0	111.2	1.1	100
22	14	376	604	0.62	0.04815	0.00161	0.11498	0.00362	0.01732	0.00015	106.6	77.0	110.5	3.3	110.7	0.9	100
23	12	361	474	0.76	0.05035	0.00195	0.11876	0.00437	0.0171	0.00016	211.1	87.2	113.9	4.0	109.3	1.0	96
24	17	523	651	0.80	0.04985	0.00124	0.11942	0.00273	0.01737	0.00012	187.9	56.9	114.5	2.5	111.0	0.8	97
25	11	258	468	0.55	0.04789	0.00151	0.11661	0.00347	0.01766	0.00014	92.9	74.2	112.0	3.2	112.8	0.9	99
26	15	440	572	0.77	0.04902	0.0014	0.11726	0.00312	0.01735	0.00013	148.6	65.6	112.6	2.8	110.9	0.8	98
27	21	616	842	0.73	0.04813	0.00129	0.11559	0.00287	0.01742	0.00013	105.5	62.2	111.1	2.6	111.3	0.8	100
28	11	320	470	0.68	0.04801	0.002	0.11385	0.00455	0.01719	0.00017	98.8	96.9	109.5	4.1	109.9	1.1	100
29	11	278	428	0.65	0.04994	0.00195	0.11803	0.0044	0.01714	0.00017	192.0	88.5	113.3	4.0	109.5	1.1	97
30	18	595	695	0.86	0.04868	0.00125	0.11764	0.00279	0.01752	0.00012	132.5	59.5	112.9	2.5	112.0	0.8	99
31	8	173	291	0.60	0.04969	0.00173	0.12056	0.00398	0.01759	0.00015	180.7	79.2	115.6	3.6	112.4	1.0	97
32	9	195	360	0.54	0.05019	0.00162	0.11967	0.00365	0.01729	0.00014	203.9	73.4	114.8	3.3	110.5	0.9	96

In the Gerze area, detrital zircon ages from the Duoni Formation range from 119–123 Ma (Li *et al.*, 2020), while igneous zircons yielded ages of *ca.* 113 Ma (Kong *et al.*, 2019).The Duoni Formation in the Baingoin area contains interbedded andesite layers with radiometric ages around 113 Ma (Zhu *et al.*, 2019, 2022). Collectively, these age data suggest that the Duoni Formation along the BN belt generally falls within a similar age range of 110–125 Ma, consistent with the broader range proposed by paleontological studies.

The Duoni Formation is widely regarded as containing sedimentary detritus resulting from the initial collision between the Qiangtang and Lhasa blocks. Particularly following several detrital provenance analyses along the BN belt, it has been proposed that the Duoni Formation has incorporated detrital material derived from the opposing blocks involved in the collision (Zhu *et al.*, 2016; Fan *et al.*, 2017; Sun *et al.*, 2017; Lai *et al.*, 2019; Chen *et al.*, 2020; Li *et al.*, 2020). Consequently, the stratigraphic age of the Duoni Formation provides critical chronological constraints on the timing of the initial collision between the two blocks. The ages of Duoni Formation from the whole belt are crucial for understanding the spatiotemporal dynamics of this collision from eastern to western regions. In this geological context, the age of the Duoni Formation in the eastern region suggests that the collision between

the two blocks may have occurred around 112–114 Ma. The analysis of detrital provenance for the Duoni Group in Basu County, in Lhasa block, also suggests that it may have received detrital material from the South Qiangtang Block (Yin *et al.*, 2024). This further implies that along the BN suture, the initial collision between the Qiangtang and Lhasa blocks occurred approximately within a similar time frame, ranging from 110 to 125 Ma, from east to west. However, further detailed provenance analysis is required to confirm whether the sedimentary detrital material of the Duoni Formation in the eastern region was sourced from the opposing terrane during the collision.

The corresponding Palaeontology in eastern Tibet

Fossil evidence initially provided age constraints for the Duoni Formation in eastern Tibet. For instance, the *Zamiophyllum-Weichselia-Klukia* assemblage, found in the lower and middle parts of the Duoni Formation in eastern Tibet (Chen *et al.*, 1983; Yang & Chen, 1983), was assigned to the Neocomian period. Additionally, the discovery of *Grammatodon carinatus* and *Lopha shadingensis* sp. in the middle part of the formation, when compared with related European fossils, suggested an Aptian–Albian age (Yang & Chen, 1983). By comparing these paleontological findings with the zircon U-Pb ages obtained in this study, ranging from 110.95–112.8 Ma, we find that these results align with the Aptian–Albian period, confirming the consistency between the two methods and refining the temporal framework for these fossils in eastern Tibet.

In comparison, paleontological evidence from the central-western segment of the Duoni Formation along the BN belt also supports an Early Cretaceous age. Foraminifera, bivalves, and ammonites collected in Baingoin County indicate an age range from the Barremian to Cenomanian and Berriasian to Valanginian periods (Zhang *et al.*, 2019). In the Xiongmei-Qusongbo area, bivalve and foraminifera fossils date to the Barremian-Aptian–Albian range (Zheng *et al.*, 2003). Additionally, spore-pollen fossils from the Duoni Formation in Jiali have been assigned to the Berriasian-Valanginian period (Yang *et al.*, 2009). In summary, the paleontological evidence from the central and western segments of the BN belt consistently points to an Early Cretaceous age, particularly within the Aptian–Albian, which aligns with findings from the eastern segment.

Conclusion

We conducted LA-ICP-MS zircon U-Pb dating on three tuff samples from the upper Duoni Formation in eastern Tibet to more precisely constrain its age. The results indicate that the top layers of the Duoni Formation in the eastern part of the BN belt is approximately 110.95–112.8 Ma, corresponding to the early Albian. This age aligns with paleontological evidence from the Duoni Formation, reflects the closure of the BN Ocean and the timing of the collision between the Lhasa and Qiangtang blocks. When compared with the western and central segments of the BN belt, the tuff rocks in the eastern part display a similar early Albian age range, consistent with paleontological findings such as the *Zamiophyllum-Weichselia-Klukia* assemblages and fossil discoveries in the central-western areas. This study fills a gap in the previous research on eastern Tibet, providing stronger constraints on both the fossil records and the sedimentary processes related to the Qiangtang-Lhasa collision. Together with previous research, these findings significantly enhance the stratigraphic understanding of the Duoni Formation along the BN belt, offering a better picture of the region's tectonic and bio-stratigraphic evolution.

Acknowledgments

We would like to express our gratitude to Xiaokai Yang, Tianhao Wu, Xinneng Lian, Xinran Li, Jian Gao, Hang Yang and Jiashuo Liu for their assistance during field work and valuable discussions, to Prof. Jianguo Li for his invaluable guidance and support during the fieldwork. This study was funded by the Second Tibetan Plateau Scientific Expedition and Research project (2019QZKK0706), National Science Foundation of China (41925008, 42272235), and the Foundation of Chinese Academy of Science (E22117).

References

Chen, F. & Yang, G. (1982) Lower Cretaceous plants from Pingquan, Hebei Province and Beijing, China. *Acta Botanica Sinica*, 24, 575–580.

Chen, J., Cao, M., Lin, Q. & Liu, X. (1983) The Jingxing fossil fauna was discovered in eastern Tibet. *Chinese Science Bulletin*, 19, 1187–1190. https://doi.org/10.1360/csb1983-28-19-1187

Chen, Y., Ding, L., Li, Z., Laskowski, A.K., Li, J., Baral, U., Qasim, M. & Yue, Y. (2020) Provenance analysis of Cretaceous peripheral foreland basin in central Tibet: implications to precise timing on the initial Lhasa-Qiangtang collision. *Tectonophysics*, 775, 228311. https://doi.org/10.1016/j.tecto.2019.228311

Fan, J., Li, C., Xie, C., Wang, M. & Chen, J. (2015) The evolution of the Bangong-Nujiang Neo-Tethys ocean: evidence from zircon U-Pb and Lu-Hf isotopic analyses of Early Cretaceous

oceanic islands and ophiolites. *Tectonophysics*, 655, 27–40. https://doi.org/10.1016/j.tecto.2015.04.019

Fan, S.Y., Ding, L., Murphy, M.A., Yao, W. & Yin, A. (2017) Late Paleozoic and Mesozoic evolution of the Lhasa Terrane in the Xainza area of southern Tibet. *Tectonophysics*, 721, 415–434. https://doi.org/10.1016/j.tecto.2017.10.022

Girardeau, J., Marcoux, J., Allegre, C.J., Bassoullet, J.P., Tang, Y.K., Xiao, X.C., Zao, Y.G. & Wang, X.B. (1984) Tectonic environment and geodynamic significance of the Neo-Cimmerian Donqiao ophiolite, Bangong-Nujiang suture zone, Tibet. *Nature*, 307, 27–31. https://doi.org/10.1038/307027a0

Hu, X., Ma, A., Xue, W., Garzanti, E., Cao, Y., Li, S.M., Sun, G. & Lai, W. (2022) Exploring a lost ocean in the Tibetan Plateau: Birth, growth, and demise of the Bangong-Nujiang Ocean. *Earth-Science Reviews*, 229, 104031. https://doi.org/10.1016/j.earscirev.2022.104031

Kapp, P., Yin, A., Harrison, T.M. & Ding, L. (2005) Cretaceous-Tertiary shortening, basin development, and volcanism in central Tibet. *Geological Society of America Bulletin*, 117. https://doi.org/10.1130/b25595.1

Kapp, P., DeCelles, P.G., Gehrels, G.E., Heizler, M. & Ding, L. (2007) Geological records of the Lhasa-Qiangtang and Indo-Asian collisions in the Nima area of central Tibet. *Geological Society of America Bulletin*, 119, 917–933. https://doi.org/10.1130/b26033.1

Kong, C., Zhang, Z., Wu, Y., Jiao, S., Cao, Y., Duan, K. & Zhi, S. (2019) Geochemical characteristics, chronology and geological significance of volcanic rocks in Duoni Formation in the north of Wuma Township,Gaize County,Tibet. *Mineral Exploration*, 6, 1304–1315. https://doi.org/CNKI:SUN:YSJS.0.2019-06-017

Košler, J. (2007) Laser ablation ICP-MS—a new dating tool in Earth science. *Proceedings of the Geologists' Association*, 118, 19–24. https://doi.org/10.1016/S0016-7878(07)80043-5

Lai, W., Hu, X., Garzanti, E., Xu, Y., Ma, A. & Li, W. (2019) Early Cretaceous sedimentary evolution of the northern Lhasa terrane and the timing of initial Lhasa-Qiangtang collision. *Gondwana Research*, 73, 136–152. https://doi.org/10.1016/j.gr.2019.03.016

Li, P. (1982) Preliminary study of early Cretaceous plant fossils from the Duoni Formation in eastern Tibet. *Stratigraphy and Paleontology of the Eastern Tibetan Plateau and Western Sichuan*, 71–105.

Li, S., Yin, C., Ding, L., Guilmette, C., Zhang, J., Yue, Y. & Baral, U. (2020) Provenance of Lower Cretaceous sedimentary rocks in the northern margin of the Lhasa terrane, Tibet: implications for the timing of the Lhasa-Qiangtang collision. *Journal of Asian Earth Sciences*, 190. https://doi.org/10.1016/j.jseaes.2019.104162

Ma, A., Hu, X., Garzanti, E., Boudagher-Fadel, M., Xue, W., Han, Z. & Wang, P. (2023) Paleogeographic and tectonic evolution of Mesozoic Qiangtang basins (Tibet). *Tectonophysics*, 862. https://doi.org/10.1016/j.tecto.2023.229957

Sun, G., Hu, X. & Sinclair, H.D. (2017) Early Cretaceous palaeogeographic evolution of the Coqen basin in the Lhasa Terrane, southern Tibetan plateau. *Palaeogeography, Palaeoclimatology, Palaeoecology*, 485, 101–118. https://doi.org/10.1016/j.palaeo.2017.06.006

Taylor, M., Yin, A., Ryerson, F.J., Kapp, P. & Ding, L. (2003) Conjugate strike-slip faulting along the Bangong-Nujiang suture zone accommodates coeval east-west extension and north-south shortening in the interior of the Tibetan Plateau. *Tectonics*, 22. https://doi.org/10.1029/2002TC001383

Wang, B., Wang, L., Chung, S., Chen, J., Yin, F., Liu, H., Li, X. & Chen, L. (2016) Evolution of the Bangong–Nujiang Tethyan ocean: Insights from the geochronology and geochemistry of mafic rocks within ophiolites. *Lithos*, 245, 18–33. https://doi.org/10.1016/j.lithos.2015.07.016

Wu, Y. (1985) The early Cretaceous Coal-bearing strata and flora in Xizang. *Contribution to the geology of the Qinghai-Xizang (Tibet) Plateau*.

Yang, S. & Chen, J. (1983) The Age of the Doni Formation from the Bivalve Fossils. *Journal of Stratigraphy*, 7, 285–288.

Yang, D., Hu, B., Dong, Q. & Wang, T. (2009) Lithostratigraphy and sedimentary environment in Lower Cretaceous Duoni Formation in Baga area of Jiali,Tibet. *Global Geology*, 28, 280–283. https://doi.org/10.1042/BSR20080061

Yin, Z., Ding, L., Li, J., He, Z., Wang, H., Wang, C., Wang, L., Zhao, C., Deng, G., Yue, Y., Xie, J. & Cai, F. (2024) The Cretaceous suturing process of the eastern Bangong-Nujiang Ocean, Basu area. *Palaeogeography, Palaeoclimatology, Palaeoecology*, 642. https://doi.org/10.1016/j.palaeo.2024.112154

Zhang, Q., Ding, L., Cai, F., Xu, X., Zhang, L., Xu, Q. & Willems, H. (2011) Early Cretaceous Gangdese retroarc foreland basin evolution in the Selin Co basin, central Tibet: evidence from sedimentology and detrital zircon geochronology. *Geological Society, London, Special Publications*, 353, 27–44. https://doi.org/10.1144/SP353.3

Zhang, Z., Luo, X., Liu, B., Wu, X. & Dai, R. (2019) Stratigraphic characteristics, formation age and sedimentary environment of the Duoni formation in Wuma Township, Gaize county, Tibet. *Mineral Exploration*, 10, 1316–1326. https://doi.org/10.1016/j.palaeo.2017.06.006

Zheng, C., Qu, Y., Zhang, S., Liu, G. & Feng, D. (2003) On the Lithostratigraphy and Sedimentary Environment of the Lower Cretaceous Duoni Formation in the Xungmai and Qusongbo Areas, Northern Xizang. *Geological Review*, 49, 638–645. https://doi.org/10.1016/S0955-2219(02)00073-0

Zhou, M., Min, N. & Wang, S. (2000) *Stratigraphy of China*. 2482.

Zhu, D., Li, S., Cawood, P.A., Wang, Q., Zhao, Z., Liu, S. & Wang, L. (2016) Assembly of the Lhasa and Qiangtang terranes in

central Tibet by divergent double subduction. *Lithos*, 245, 7–17.
https://doi.org/10.1016/j.lithos.2015.06.023

Zhu, Z., Zhai, Q., Hu, P., Chung, S., Tang, Y., Wang, H., Wu, H., Wang, W., Huang, Z. & Lee, H. (2019) Closure of the Bangong-Nujiang Tethyan Ocean in the central Tibet: Results from the provenance of the Duoni Formation. *Journal of Sedimentary Research*, 89, 1039–1054.
https://doi.org/10.2110/jsr.2019.55

Zhu, Z., Zhai, Q., Hu, P., Tang, Y., Wang, H., Wang, W., Wu, H. & Huang, Z.Q. (2020) Timing of the Lhasa-Qiangtang Collision: Constraints from the sedimentary records of the Duoni Formation from the middle segment of the Bangong-Nujiang suture zone. *Acta Sedimentologica Sinica*, 38, 712–726.
https://doi.org/10.14027/j.issn.1000-0550.2019.081

Zhu, Z., Zhai, Q., Hu, P., Tang, Y., Wang, H., Wang, W. & Wu, H. (2022) Resolving the timing of Lhasa-Qiangtang block collision: Evidence from the Lower Cretaceous Duoni Formation in the Baingoin foreland basin. *Palaeogeography, Palaeoclimatology, Palaeoecology*, 595.
https://doi.org/10.1016/j.palaeo.2022.110956